Journal of Polymers and the Environment (2020) 28:532–541
https://doi.org/10.1007/s10924-019-01610-z

ORIGINAL PAPER

Boric Acid Cross-linked 3D Polyvinyl Alcohol Gel Beads by NaOH-Titration Method as a Suitable Biomass Immobilization Matrix

Li Sun[1] · Jinxing Wang[1] · Jidong Liang[1,2] · Gaigai Li[1]

Published online: 7 December 2019

Abstract
Granule-base immobilization of biomass is a potential method for a decent quality granular sludge cultivation. In this study, 3D polyvinyl alcohol (PVA) gel beads were chemically cross-linked via a simple NaOH-titration method. The PVA gel beads' porous morphology was characterized using scanning electron microscope (SEM) and Brunauer–Emmette–Teller (BET), and their mechanical properties were evaluated by swelling rate and compressive stress tests. When cross-linking time was 10 min, high quality gel beads (P10) were synthesized, which demonstrated a homogeneous porous structure, good swelling rate, and high compressive strength. A mechanism for synthesis of the gel beads was proposed based on the results of Fourier transform infrared (FTIR) and X-ray diffractometer (XRD) analysis. Briefly, the intermolecular hydrogen bonds of PVA were firstly broken by NaOH to generate active bond of O–Na, which easily reacted with $B(OH)_4^-$ to produce the PVA-boric acid gel beads. P10 showed excellent biocompatibility for anaerobic ammonia oxidation (anammox) biomass' immobilization. After incubation for three months, well granule-base immobilized sludge on P10 was developed in up-flow reactor. The sludge had high abundance of anammox biomass and was in balance with other functional bacteria. This work provides a simple method for the rapid preparation of 3D PVA gel beads and verifies their potential in granule-base immobilization of biomass.

Keywords Polyvinyl alcohol · Boric acid · Cross-linking · Gel beads · Immobilization

Introduction

Carrier-assisted immobilization of biomass is a promising strategy for improving the performance of wastewater treatment bioreactors [1–3]. Compared with suspended active sludge, granule-base immobilized sludge with carriers is beneficial for biomass retention as carriers can provide a good habitat for attach-growth and proliferation of microbes and also help the microbes in resisting the impact of harsh environmental conditions [4].

Several natural and synthetic polymers such as polyacrylamide, sodium alginate, agar, and polyvinyl alcohol (PVA) have been used for biomass immobilization [5, 6]. Among these, PVA is a good candidate to synthesize carriers for biomass immobilization because PVA is biocompatible and slowly degradable [7, 8]. Usually, PVA biological carriers are prepared by physical cross-linking and chemical cross-linking technique. Physical crosslinking usually adopts freeze-thawing cycle method, which refers to the process of using hydrogen bonds within PVA molecules, microcrystalline regions, and entanglement links between the macromolecular chains, and forming a three-dimensional network through hydrophobic action [9]. For instance, Zhang et al. successfully immobilized *Methanosarcina* bacteria in the PVA gel beads that were prepared by freeze-thawing method, and the UASB (Up-flow anaerobic sludge bed) reactor consisting of these gel beads could achieve the biomass attachment of 0.93 g VSS/g [10]. Wang et al. immobilized *Clostridiaceae bacterium, Alpha proteobacterium,*

Li Sun and Jinxing Wang have contributed equally to this work.

Electronic supplementary material The online version of this article (https://doi.org/10.1007/s10924-019-01610-z) contains supplementary material, which is available to authorized users.

✉ Jidong Liang
jidongl@xjtu.edu.cn

[1] Department of Environmental Science and Engineering, Xi'an Jiaotong University, Xi'an 710049, China

[2] Department of Environmental Technology, Wageningen University, Wageningen, Netherlands

Phenylobacterium haematophilum, and *Rhodobacter* on the PVA-based gel beads formulated by freezing-and-thawing cycle method, which greatly enhanced the stability of a moving bed biofilm reactor system [6].

However, PVA biological carrier prepared by repeated freeze-thawing cycle method requires large refrigeration equipment, leading to high energy consumption and long production cycle, and the carrier has large water-soluble swelling property, which limit its applications [11]. Thus, chemical cross-linking method is a promising economical method for preparation of PVA gel beads. In general, boric acid is used as a cross-linking reagent for synthesis of PVA gel. Boric acid, a non-toxic material, is considered as a Lewis acid (electron acceptor) with an empty p orbital that can be attracted to hydroxyl groups in the PVA molecules to achieve chemical cross-linking [12]. In PVA-boric acid reaction, boric acid acts as the cross-linker, and the hydroxyl groups on PVA are linked by boron. Consequently, monodiol-type of gel lattice of PVA-boric acid is produced [13]. The PVA-boric acid method is considered as a gentle synthesis procedure as no toxic agents are used to prevent biological inhibition [14]. Besides, PVA-boric acid materials display good water, oxygen, and shear resistance [15–17]. Therefore, PVA-boric acid method has broad applications in the preparation of biocarriers. However, the currently employed PVA-boric acid crosslinking method is slow (more than 18 h), which results in difficulty in shaping of products and ease of adhesiveness [18]. Meanwhile, with the increase in cross-linking duration, a dense layer is usually formed on the surface of the products, which limits the mass transfer and results in drawbacks in applications [19]. For example, for gas producing biomass (such as methanogens, hydrogenogens, anaerobic ammonia oxidation (anammox) bacteria, denitrifiers, etc.), biogas blocked inside the granular sludge can lead to a high pressure that can destroy the granules [20]. Therefore, to develop ideal and quick PVA gel beads, synthesis method is significant to overcome the above mentioned problems [21].

In this work, a simple method to rapidly fabricate 3D PVA gel beads with homogeneous porous structure was developed. The method can be specified in simpler terms as NaOH-titration method by injecting alkali PVA solution into the saturated boric acid solution with 1% of calcium chloride ($CaCl_2$). The preparation process was quick and environmental friendly. The ideal biocarriers employed in wastewater treatment reactors should meet two basic requirements: (1) biocompatible and porous for cells accommodation; (2) appropriate mechanical strength to resist hydraulic forces. Therefore, in this study, the characteristics of the synthesized 3D PVA gel beads were evaluated using Scanning electron microscope (SEM), Brunauer–Emmette–Teller (BET), swelling rate test, and compressive stress test. Also, the synthesis mechanism is proposed based on the results of Fourier transform infrared (FTIR) and X-ray diffractometer (XRD). Finally, the biomass granule immobilization of the gel beads was investigated in an UASB (up-flow anaerobic sludge bed/blanket) reactor by using anammox bacteria as example. To the best of our knowledge, it is the first time that such a simple method for PVA gel beads quick preparation without any supporting materials is presented and their application in granule-base immobilization of anammox biomass assistance is discussed. The work would be beneficial for the development of 3D PVA gel beads synthesis and promote wastewater treatment upgrading.

Materials and Methods

Chemicals

Polyvinyl alcohol (PVA) (the degree of polymerization is 2488) was obtained from Kaiyuan Chemical Technology Co., Ltd., China. Boric acid (99.9%), NaOH, $CaCl_2$, and other chemicals were purchased from Tianjin Fuchen Chemical Reagent Co., Ltd., China. All the chemicals were of analytical grade. The ultra-pure water was obtained from an UPT-II-10 T system (Chengdu super pure water technology Co., Ltd., China).

NaOH-Titration Method for PVA Gel Beads Preparation

PVA solution was prepared by completely dissolving 12.0 g of PVA polymer powder in 100 mL of deionized water and stirring for 1 h under 85 ℃ to form homogeneous PVA solution. Then, the solution was stewed a moment at room temperature, which was followed by addition of 5% NaOH solution (1.5 g of NaOH dissolved in 30 mL deionized water) to the above PVA solution, obtaining alkali PVA solution. Thereafter, ultrasonication was used to remove bubbles from the alkali PVA solution. Then, the alkali PVA solution was added dropwise into the cross-linking agent (saturated boric acid solution containing 1% $CaCl_2$) via a peristaltic pump (BT-100, Baoding Lange constant flow pump Co., Ltd., China) equipped with a Lange tube (ID 0.5 mm). The spherical beads were formed and stirred magnetically. The spherical PVA beads were labeled as P5, P10, P15, P25, and P30 according to the different cross-linking times (5 min, 10 min, 15 min, 25 min, and 30 min), respectively. The gel beads were taken out carefully and washed with deionized water till pH was neutral. The preparation process is presented in Supplementary Fig. S1.

Characterization of 3D PVA Gel Beads

Micromorphology and the Specific Surface Area

Scanning electron microscope (SEM, Quanta-200, USA) was used for micromorphology observations of the PVA gel beads at an accelerating voltage of 15 kV. The samples were

freeze-dried using liquid nitrogen. All these gel beads were sputter-coated with gold layer for 90 s before measurements.

The specific surface area of different gel beads was calculated as per the static volumetric method with the Brunauer–Emmett–Teller (BET) equation by using JW-BK200B specific surface analyzer (China) at 77 K. Before measurements, the samples were freeze-dried for 24 h to remove water and degassed for 2 h at room temperature in vacuum.

Swelling Rate and Compressive Stress Test

Swelling rate was determined by the gravimetric method. Dry PVA gel beads were weighed on an analytical balance (Quintix125D-1CN, SARTORIUS, Germany) and recorded as Wd (g). Then, the dry PVA gel beads were immersed in 200 mL deionized water and stored at 33 ℃ by using a thermostate chamber. After particular time intervals, the residual water was withdrawn using the paper filter, and the samples were weighed and recorded as We (g). The swelling ratio was determined until the weight of the gel beads was constant. The swelling rate can be calculated as follows:

$$\text{Swelling rate } (\%) = \frac{We - Wd}{Wd} \times 100\% \quad (1)$$

The compression strength of the 3D PVA gel beads was measured as per ISO527-3-1995 (E) using a dynamic thermo-mechanical analyzer (DMA 242E, Netzsch, Germany) at the environmental temperature. The loading rate was 1 mm/min while the frequency was 1 Hz. Five specimens for each sample were measured as per the ASTM D 1708 standard. As the strength data are related to ambient temperature and humidity, they were obtained under the same conditions.

FTIR and XRD Analyses

The functional groups of PVA, alkali PVA, and the selected 3D gel beads (P10 and P15) were identified with FTIR spectrometer (Nicolet NEXUS 750, USA) at the spectral resolution of 4 cm^{-1} in range of 400–4000 cm^{-1}. Before measurements, the samples were freeze-dried, milled into powder, and mixed with KBr.

X-ray diffraction (XRD) of PVA, alkali PVA, and the selected 3D gel beads (P10 and P15) were analyzed with a Bruker D8 ADVANCE X-ray diffractometer (Holland). The samples were analyzed with Cu-Kα radiation after freeze–thaw and scanned in the range of diffraction angle 2θ = 10–90° at an angular speed of 0.03°/s.

Granule-Base Immobilization of Biomass

Reactor Operation

An UASB reactor was operated for three months under 33 ℃ in a thermostat chamber for incubating the granule-base immobilization of biomass by 3D PVA gel beads.

First, the reactor was inoculated with 50 mL P10 and 500 mL seed sludge. The seed sludge was taken from another UASB reactor for anammox system, which had been operated for about 300 days with a working volume of 2.5 L and the nitrogen removal efficiency (NRE) of this reactor was approximately 90% with a relatively high nitrogen loading rate (NLR) (10.46 kg-N m^{-3} d^{-1}). The reactor was continuously fed with synthetic influent by peristaltic pumps at the flow rate of 51.67 L d^{-1}. The influent contained: NH_4^+-N (4.20–150) mg L^{-1}, NO_2^--N (5.40–165) mg L^{-1}, $CaCl_2$ 135 mg L^{-1}, $MgSO_4$ 146 mg L^{-1}, KH_2PO_4 27 mg L^{-1}, $KHCO_3$ 500 mg L^{-1}, and 1 mL trace element solution [22]. pH of the influent was adjusted to 7.0 ± 0.2 by the addition of 1 mol L^{-1} NaOH or HCl solution, and then purged by N_2 for more than 20 min daily to keep the dissolved oxygen levels below 0.5 mg L^{-1}.

SEM Analysis of the Incubated Granular Sludge

The morphologies of the initial and final granule-base immobilized sludge were analyzed using a thermally assisted field Scanning Electron Microscope (SEM, Quanta-200, USA). The samples were gently fixed with 2.5% (v/v) glutaraldehyde for 2–12 h at 4 ℃, and then, washed with 0.1 M phosphate-buffered saline (PBS) (pH 6.8) for three times (10 min at each time). Afterwards, the samples were dehydrated in a graded ethanol series (30, 50, 70, 90, and 100%, 15 min per step). Then, isoamyl acetate mixed with ethanol in a ratio of 1:1 was applied to achieve metathesis of ethanol in the samples (15 min). Lastly, the samples were placed in a simple desiccator and incubated for about 4 h for imaging under SEM at an accelerating voltage of 15 kV.

Microbial Diversity of the Incubated Granular Sludge

High-throughput 16S rRNA sequencing was employed for microbial diversity analysis. 0.5 g of wet sludge pellet was collected for DNA extraction with D5625-01soil DNA kits (Omega, USA). Then, the qualified DNA was amplified by PCR using primer set 341F and 805R for the V3–V4 region of the 16S rRNA. Then, high-throughput pyrosequencing was performed on a MiSeq Illumia platform (Sangon Biotech, Co., Ltd., Shanghai, China). The RDP classifier was used to classify the species units of each sequence. The

sequence abundance of each sample and each species unit was calculated, and the species taxon and sample abundance table were constructed.

Results and Discussion

Morphologies and Porous Structure of PVA Gel Beads

The images of the PVA gel beads with different cross-linking times (noted as P5, P10, P15, and P30) are shown in Supplementary Fig. S2. All the PVA gel beads exhibited good formability and smooth appearance with diameters of 3–5 mm. With the increase in chemical cross-linking time, the gel beads gradually changed from a circle-layer (P5 and P10) structure to a core–shell structure (P15 and P30). After 15 min, the gel beads as a core–shell structure was developed, and the shell and core could be completely separated.

SEM images were taken for inspecting the surface (Fig. 1a–d) and the cross-sectional (Fig. 1a′–d′) morphologies of the PVA gel beads. Both the surface and cross section of P10 displayed homogeneous and well-developed pores. Apparently, the pores in the surface of P5 were inhomogeneous as compared with P10. As the cross-linking reaction proceeded, dense layer began to appear on the surface of P15 and P30, which may have led to a decrease in the diffusion flux of the crosslinking agent and slow down the internal crosslinking reaction, resulting in a reduction of the internal pores and a tight package. In other words, the inconsistency of the internal and external crosslinking degree due to different diffusion velocities of the crosslinking agent resulted in the separation of the core and the shell (see Supplementary Fig. S2). Previous studies have also indicated the presence of dense layers when PVA was cross-linked with boric acid [23].

According to BET results (Table 1), the specific surface area of P5 was only 0.28 m^2/g, while those of P10, P15, and P30 were 4.50 (1.26 m^2/g), 3.57 (1.00 m^2/g), and 2.32 (0.65 m^2/g) times that of P5, respectively. The results suggest that specific surface area of PVA gel beads increase with the development of the cross-linking reaction but decrease when the cross-linking progress to a certain stage. However, as the cross-linking reaction progressed (from 10 to 30 min), the surface area of P15 and P30 became smaller owing to their closed-surface morphology, which is consistent with the SEM observations.

Combining the evidence from SEM and BET results, when the cross-linking reaction occurred, PVA matrix began to change and formed an internally and externally developed pore structure, which led to an increase in the specific surface area. However, with further increase in cross-linking duration, the gel beads loose the regular structure and gradually form a dense layer in the outer layer, resulting in the reduction of specific surface area. Among all the gel beads synthesized in this study, P10 displayed the maximum specific surface area and the best uniform porous structure, and can provide a good matrix for biomass attach-growth and be beneficial for the transmission of substrates. All these properties are advantageous for their application as biocarriers for biomass immobilization.

Swelling Rate and Mechanical Properties of the PVA Gel Beads

Figure 2a shows the swelling ratio of the PVA gel beads with different cross-linking times. The maximum swelling ratio of the different PVA gel beads was 225.26% (P5), 351.96% (P10), 345.31% (P15), and 305.83% (P30), respectively. P10 exhibited the largest swelling capacity. The pore size and porosity of PVA gel beads were the primary factors affecting the swelling degree. Short cross-linking duration may not be enough for forming complete networks to accept water (such as in the case of P5). But long cross-linking times resulted in tight networks, which limited the water-absorbing capacity (such as in the case of P30).

At a low cross-link density, the pores had not yet been completely developed (as shown in Supplementary Fig. S3). The diffusion of water into the shrunken pores was extremely difficult, resulting in a low degree of equilibrium expansion [24]. The increase in degree of swelling was slightly smaller at larger cross-linking ratio because of the larger number of chemical cross-links per unit volume of gel, which may lead to too tight networks to provide water-absorbing capacity (such as in the case of P30) [25]. Also, longer the cross-linking reaction, more regular is the arrangement of hydrogen bonds in the molecules, which would create obstacles for entry of water, and finally, reduce their swelling ratio [20]. As found in our study, the swelling of each kind of gel beads stabilized ultimately and no longer increased with time. High swelling rate of gel beads was induced by the elasticity of the network [26]. Therefore, the swelling properties of the gel beads are important when they are used as filling materials in the high flow rate reactors. In this case, PVA gel beads with high swelling rate can be compressed without any mechanical destruction caused by fluent shear action.

Figure 2b shows the compressive stress–strain curves of the PVA gel beads. Clearly, P10 and P15 exhibited higher compressive strengths (0.29 MPa and 0.32 MPa) than P5 and P30 (0.21 MPa and 0.15 MPa). Notably, the compressive strength of P15 and P30 were dramatically increased when the strain was above 70%. As also reported in literature [25], the phenomenon might be caused by the formation of core–shell structure when the crosslinking time was 15 min. When the strain was higher than 70%, the shell

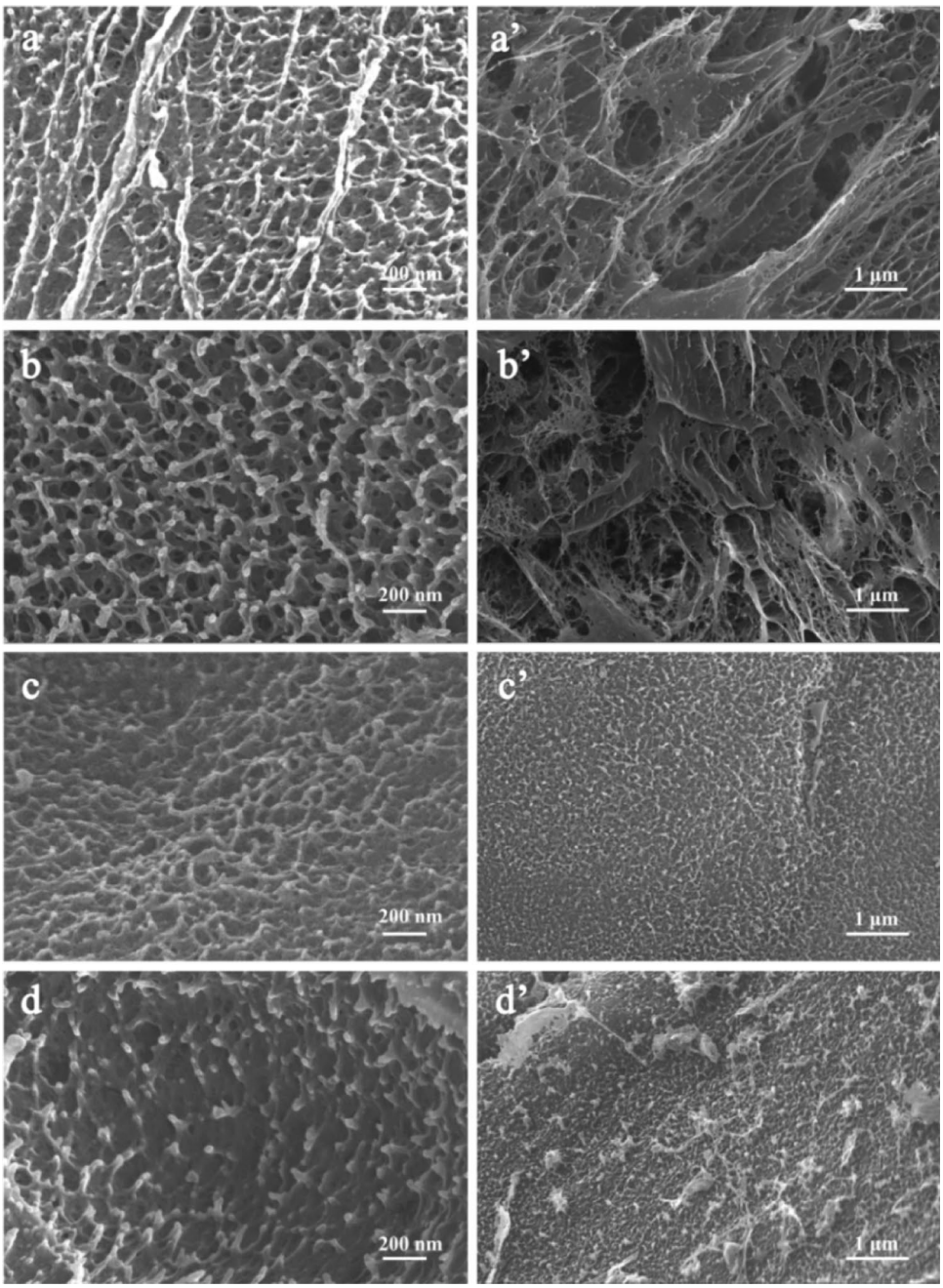

Fig. 1 SEM images of the surface of P5 (**a**), P10 (**b**), P15 (**c**), P30 (**d**) gel beads, and the cross-section for P5 (**a′**), P10 (**b′**), P15 (**c′**), P30 (**d′**) gel beads

Table 1 The specific surface area of the dried P5, P10, P15, P30 gel beads

Samples	P5	P10	P15	P30
Surface area (m^2/g)	0.28	1.26	1.04	0.65

was broken and the pore structure of the shell core was different, which might have a great effect on the compressive strength. The compressive stress is associated with the mechanical strength [23]. The denser networks and more uniform well-developed pores in the gel beads, lead to a better mechanical strength. This phenomenon can explain the higher mechanical strength of P10 and P15, which was about two folds than that of P30, as indicated by Wu et al. [27]. The high strength ensured that a large external load is required to crush the gel beads. The degree of the separation of shell and core increased with cross-linking time, which led to a decrease in the cross-linking points and weakened the compressive strength. The high mechanical strength of gel beads as carriers is of considerable interest for biomass immobilization, which can support them enduring high hydraulic shear when employed in bioreactors [28]. Therefore, P10 and P15 with high swelling

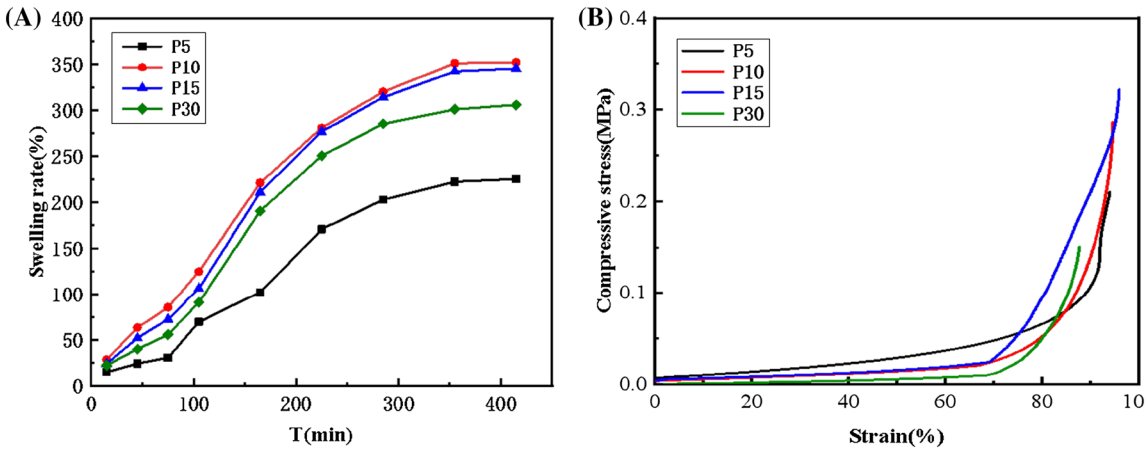

Fig. 2 Swelling rate (**a**) and compressive stress curves (**b**) of the P5, P10, P15, P20, P30 gel beads

ability as well as good mechanical properties are promising carriers for bacteria immobilization.

FTIR and XRD Analysis of PVA Gel Beads

FTIR spectra of pure PVA powder (a), Alkali PVA (b), P10 (c), and P15 (d) were obtained to identify the change in functional groups before and after the cross-linking process (Fig. 3a). For pure PVA (Fig. 3a), the most evident characteristic peak was the symmetric stretching vibrations of O–H centered at 3278 cm^{-1} [29]. The C–O stretching of the crystalline and amorphous area of PVA was at 1144 and 1096 cm^{-1}, respectively. The C–C stretching vibrations for the amorphous sequence of PVA were located at 848 cm^{-1}, and the absorption corresponding to the C–H stretching occurred at 1376 cm^{-1} [30]. Absorption bands around 1740, 1558, and 1260 cm^{-1} respectively corresponded to C=O, C=C, and C–O–C in the remaining acetyl groups from the precursor polymer of PVA [31].

Compared with FTIR of pure PVA, the spectra of alkali PVA (Fig. 3b) demonstrated that the absorbance peak of C–H shifted to higher wavenumber (from 1376 to 1414 cm^{-1}), which can be attributed to the formation of sodium alcoholate structure in PVA as described in Eq. (2). Moreover, the band at 945 cm^{-1} derived from O–H out-of-plane deformations left shifted to 924 cm^{-1} with the incorporation of NaOH solution. The shift to low wave number indicates that the intermolecular hydrogen bonds in PVA were weakened, which may be because the incorporated inclusions (NaOH) strongly interacted with the PVA molecules; thus, interfering with the interactions among PVA molecules [32]. Furthermore, the bending band from O–Na groups located at 649 cm^{-1} also showed important difference, which suggests that more cross-linking points are available for further reactions. The absorption peak at

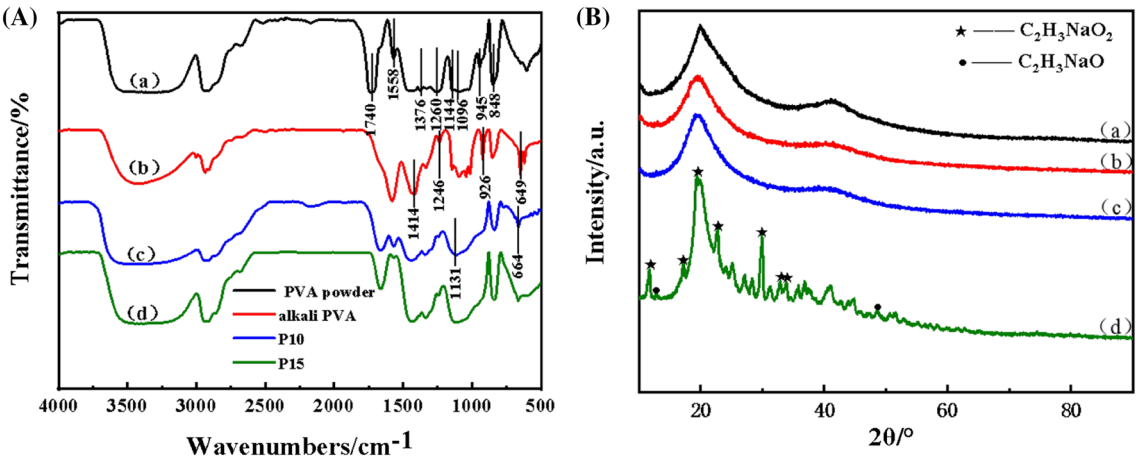

Fig. 3 FTIR (**A**) of the PVA powder (a), alkali PVA (b), P10 (c), P15 (d) and XRD (**B**) of the PVA powder (a), P10 (b), P15 (c), alkali PVA (d)

1740 cm^{-1} (C=O) disappeared, indicating that NaOH as a catalyst converted polyvinyl acetate to polyvinyl alcohol, as shown in Eq. (3). And this phenomenon was further confirmed by the shifting of the absorption bands of C–O–C from 1260 to 1246 cm^{-1}.

With the addition of boric acid, two novel peaks at 1131 cm^{-1} and 664 cm^{-1} appeared, which can be attributed to the B–O–C bending and –O–B–O stretching, respectively, and the O–Na bond at 649 cm^{-1} disappeared. The results confirm that the formation of O–Na was the key preprocess for next cross-linking reaction and could accelerate $[B(OH)_4]^-$ reaction with the hydroxyl groups in PVA chains. A few previous studies have proved that boric acid is a Lewis acid, and when alkalinity is greater than pH of 9, a compact hydrogel network is formed through the chemical bonds between $B(OH)_4^-$ and hydroxyl groups [33]. There was a decrease in intensity of peaks at 1144 and 1096 cm^{-1}, indicating that the crystallinity of PVA was modified by the interaction between PVA matrix and boric acid in the crystalline domains of PVA [20].

Typical XRD patterns of PVA powder (a), P10 (b), P15 (c), and alkali PVA (d) were investigated and their crystal degrees and crystal structures were recorded (as shown in Fig. 3b). PVA powder exhibited an extremely strong characteristic peak around 20°. In the case of alkali PVA, the novel diffraction peaks of $C_2H_3NaO_2$ and C_2H_3NaO appeared, suggesting that NaOH improved the purity of PVA. Meanwhile, the sodium alcohol structure in alkali PVA was more convenient for their cross-linking with boric acid as compared to PVA. These results are consistent with those of FTIR. After cross-linking, the above-mentioned characteristic peaks disappeared, indicating the structure transition from crystal to amorphous [34]. Such a decrease in the total crystallinity can be considered to be a vital factor in decreasing the brittleness and improving the mechanical properties of the PVA gel beads [35]. Moreover, the diffraction peaks of P10 and P15 were more broadened. These results imply that the chain alignment of PVA turned to be more disordered after cross-linking with boric acid [32].

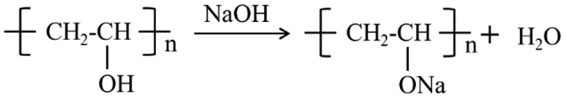

(2)

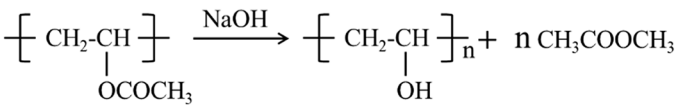

(3)

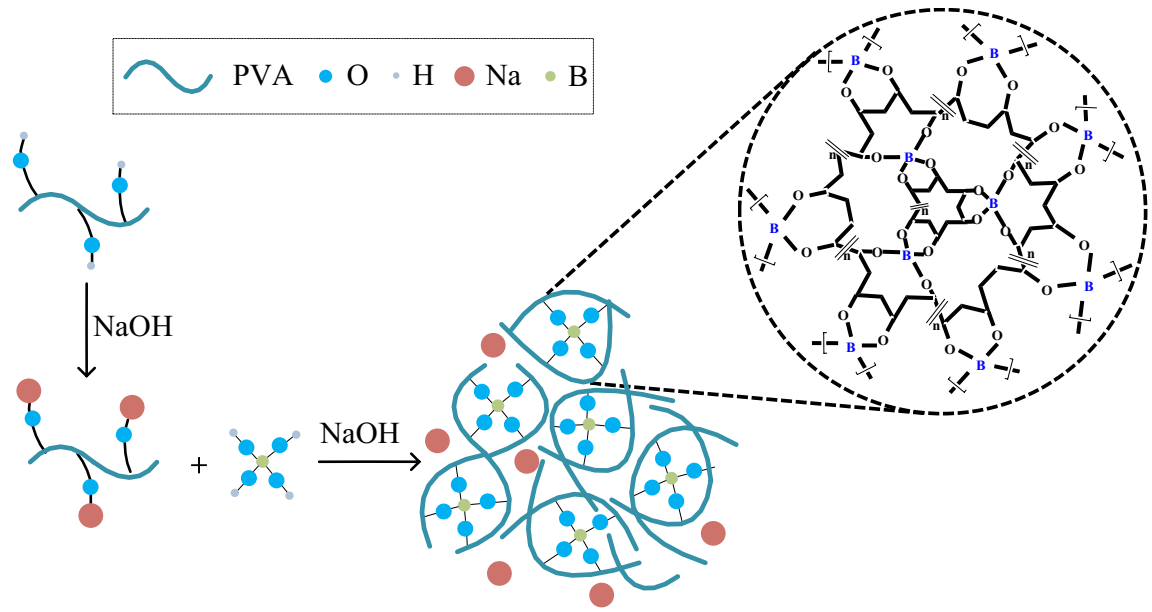

Fig. 4 The schematic diagram of the possible cross-linking reaction between PVA and boric acid

Combining the results of FTIR and XRD, we proposed the synthesis mechanism of 3D PVA gel beads by the NaOH-titration method (shown in Fig. 4). In the first step, PVA was pretreated with NaOH to produce alkali PVA, wherein the -OH of PVA changed into –O–Na. For aqueous PVA solutions, the hydrogen bonds not only bridge the PVA chains with water molecules but also bridge the inter-penetrating chains of PVA. The addition of NaOH is expected to partially deprotonate PVA and reduce the inter-chain hydrogen bonds [36]. Thus, when mixed with NaOH, the hydrogen bonds were broken by NaOH to generate O–Na, which provided more convenience for cross-linking with boric acid than OH. This theory can explain the fast cross-linking reaction for forming rigid and good spherical gel beads [37]. On the other hand, the aqueous solutions containing NaOH and PVA are beneficial for producing a tough and rubbery gel with good swelling property [38].

During the cross-linking reaction, when alkali PVA was dropped into boric acid solution, the bonds of O–Na reacted with boric acid to form stable covalent bond. Under alkaline conditions, the ortho-boric acids were hydrolyzed to $B(OH)_4^-$. When $B(OH)_4^-$ is contacted with O–Na, O–B–O is produced by losing NaOH to compact a well crosslinked PVA-boric acid layer [39]. The O–Na structure of alkali PVA performs complexation with boron atoms and rapidly shrinks to form hydrogel net. Thus, chemical bonds were established and uniformly shaped spherical beads were formed. Thereafter, the boric acid gradually penetrated into the droplet, while the cross-linking reaction continued inside the droplet, and finally, viscid and hydrophilic gel beads were formed.

Granule-Base Immobilization of PVA Gel Beads

As per the properties of the gel beads described above, P10 with uniform pore and mechanical stability was selected as biocarrier for anammox biomass granule-based immobilization. After three months of cultivation, spherical bacteria (like volcanic stone), 1 μm in diameter and loosely aggregated as micro-clusters, occupied on P10 (as shown in Fig. 5a). The colony was consistent with the characteristics of anammox bacteria culture [40], indicating that anammox bacteria successfully attach-growth and proliferated on P10 after 3 months cultivation. Thus, the PVA gel beads could provide a good habitat for bacteria in the process. Based on previous research [41], the surface bacterial polymer of carriers was mainly composed of anammox and extracellular

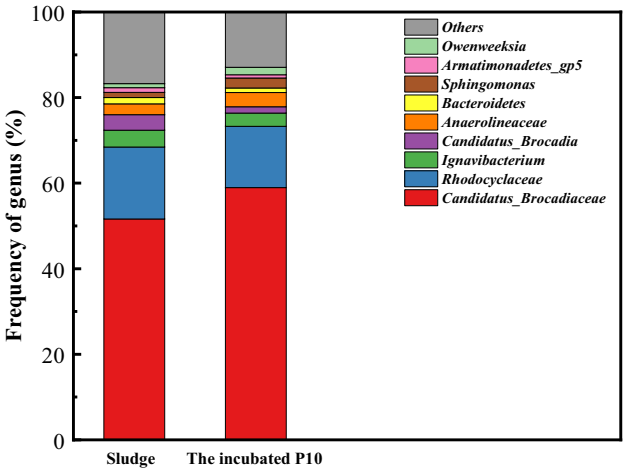

Fig. 6 The taxonomic results in genus level of sludge and the incubated P10. (Genus with ≥ 1% relative abundance in at least one sample are shown. All remaining taxa are indicated as "Others")

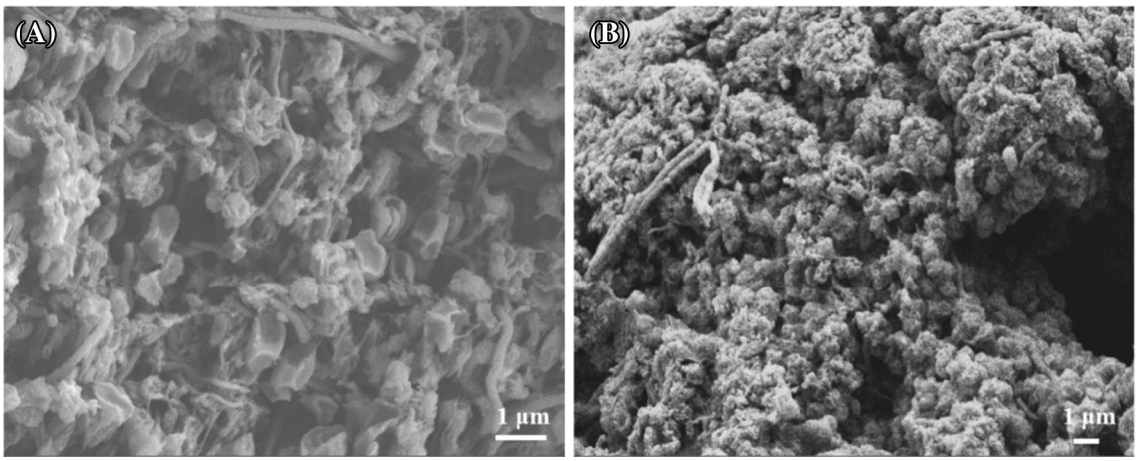

Fig. 5 SEM images of granular sludge cultured on P10

polymeric substances (EPS) which facilitated the adherence of anammox. Hence, that part of the anammox reaction was stable, which is consistent with the results of this study (as shown in Fig. 6b).

As per the results of high-throughput 16S rRNA pyrosequencing (Fig. 6), the granule-base immobilized sludge on P10 showed a similar microbial community with seed sludge, wherein the *Candidatus_Brocadiaceae* belonging to typical anammox bacteria showed the most abundance. However, the abundance of *Candidatu_Brocadiaceae* increased from 52 to 59% after 3 months cultivation. *Candidatus_Brocadiaceae* can make major contribution to the anammox process as reported earlier [42]. Therefore, it can be concluded that P10 is beneficial for enriched growth of *Candidatus_Brocadiaceae*. On the contrary, the abundance of subdominant bacteria *Rhodocyclacea* decreased from 16 to 14% after 3 months incubation. However, the abundance of *Anaerolineae* and *Ignaviboric acidcteria* genues, which have been regarded as fermentative bacteria and cooperated with anammox bacteria to remove nitrogen by a co-metabolic process in a highly enriched anammox biomass, more or less remained after three months incubation [43]. Previous studies have shown that *Anaerolineae* play an important role in the microbial granulation process and is able to remove organic carbon produced by the cell lysis [44]. *Ignavibacteria* has been verified as polysaccharides scavenger in an anammox reactor [45]. Other genus, such as *Candidatus_Brocadia* (anammox bacteria), *Bacteroidetes* (anammox bacteria), *Sphingomonas*, *Armatimonadetes_gp5,* and *Owenweeksia* changed little and also grew well on the immobilized granules.

In conclusion, P10 showed good biocompatibility to provide a favorable habitat for anammox bacteria to attached growth. Also, P10 formed a well-distributed network with high porosity, which both facilitated the substrate diffusion and benefit the adherence of anammox bacteria.

In practical applications, anammox process showed drawbacks of slow start-up and vulnerable operation, as anammox bacteria's slow growth (doubling time is 10–14 days), is accompanied with low retention of sludge in reactors caused by the wash out. Therefore, granu-base immobilization of anammox biomass is a promising approach to overcome this problem [39, 40]. After three months operation, P10 remained intact, which confirmed that the gel beads had high mechanical strength and resistance to damage, and thus, satisfy the meets of up-flow reactors.

Conclusions

3D PVA gel beads, with homogeneous porous structure, great mechanical strength, and excellent biocompatibility were prepared by the NaOH-titration method. The synthesis mechanism of the 3D PVA gel beads can be concluded in two steps. First, NaOH in PVA solution unlocked the intrinsic cross-linking hydrogen bonds in the PVA chains to produce alkali PVA with active bond of O–Na. Secondly, when the alkali PVA dropped in the boric acid solution, cross-linking reaction developed from outside of the droplet into inside and formed cross-link networks by bonds of O–B–O. When cross-linking time was set as 10 min, high quality gel beads (P10) with homogeneous porous structure, better swelling rate, and high compressive strength were produced. P10 showed excellent biocompatibility for anammox biomass. After three month operation of the bioreactor that was supplemented with P10, well-developed granular sludge was successfully incubated, which showed a high abundance of anammox biomass, keeping in balance with the other associated bacteria. In conclusion, a simple NaOH-titration method for quick preparation of PVA gel beads was developed, and the 3D PVA gel beads showed promising applications in granule-base immobilization of biomass for wastewater treatment.

Acknowledgements This study was supported by the National Natural Science Foundation of China (Grant No. 31670510) and The Key Research and Development Program of Shaanxi Province in China (2019GY-154).

Compliance with ethical standards

Conflict of interest The authors declare that they have no conflict of interest.

References

1. Gopi KM, Pakshirajan K, Das G (2018) J Environ Manag 218:486
2. Lu Y, Ma L, Liang Y, Shan B, Chang J (2018) Pol J Environ Stud 27(2):773
3. Zain NAM, Suhaimi MS, Idris A (2011) Process Biochem 46(11):2122
4. Herrero M, Stuckey DC (2015) Chemosphere 140:119
5. Gani KM, Singh J, Singh NK, Ali M, Rose V, Kazmi AA (2016) Water Sci Technol 73(7):1511
6. Wang Y, Liu Y, Feng M, Wang L (2018) J Water Reuse Desalin 8(3):340
7. Jia YG, Jin J, Liu S, Ren L, Luo J, Zhu XX (2018) Biomacromol 19(2):626
8. Song M, Yu H, Gu J, Ye S, Zhou Y (2018) Int J Biol Macromol 113:171

9. Figueroa-Pizano MD, Velaz I, Penas FJ, Zavala-Rivera P, Rosas-Durazo AJ, Maldonado-Arce AD, Martinez-Barbosa ME (2018) Carbohydr Polym 195:476
10. Wenjie Z, Dunqiu W, Yasunori K, Taichi Y, Li Z, Kenji F (2008) Bioresour Technol 99(17):8400
11. Wang JX, Liang JD, Sun L, Gao S (2019) Chemosphere 219:130
12. Soltani M, Shetab-Boushehri SF, Mohammadi H, Shetab-Boushehri SV (2013) J Med Hypotheses Ideas 7(1):21
13. Braz GHR, Fernandez-Gonzalez N, Lema JM, Carballa M (2019) Chemosphere 222:323
14. Bae H, Choi M, Chung YC, Lee S, Yoo YJ (2017) Chem Eng J 322:408
15. Dave R, Madamwar D (2006) Process Biochem 41(4):951
16. Idris A, Zain NAM, Suhaimi MS (2008) Process Biochem 43(4):331
17. Long Z, Huang Y, Cai Z, Cong W, Ouyang F (2004) Process Biochem 39(12):2129
18. Deng L, Huang B, Zhao H, Du J, Gao L (2013) Adv Mater Res 634:280–285
19. Xu X, Zhou H, Chen X, Wang B, Jin Z, Ji F (2019) Chemosphere 223:140
20. Chen C, Chen Y, Xie J, Xu Z, Tang Z, Yang F, Fu K (2017) Prog Org Coat 112:66
21. Kim JH, Rene ER, Park HS (2008) Bioresour Technol 99(3):583
22. Zhang L, Narita Y, Gao L, Ali M, Oshiki M, Okabe S (2017) Water Res 116:296
23. Wang C, Liu S, Xu X, Zhang C, Wang D, Yang F (2018) Chemosphere 203:457
24. Xue B, Deng J, Zhang J (2016) RSC Adv 6(9):7653
25. Bai H, Li Z, Zhang S, Wang W, Dong W (2018) Carbohydr Polym 200:468
26. Skouri R, Schosseler F, Munch JP, Candau SJ (1995) Macromolecules 28:197
27. Wu X, Wang H, Liu C, Zhu Z (2011) Soft Matter 7(2):579
28. Wang M, Li J, Li W, Du Z, Qin S (2018) Int J Biol Macromol 118:41
29. Shawgi N, Li S, Wang S, Li Y, Ramzi R (2018) Ceram Int 44(8):9887
30. Massoumi B, Jafarpour P, Jaymand M, Entezami AA (2015) Polymer Int 64(5):68
31. Prosanov IY, Abdulrahman ST, Thomas S, Bulina NV, Gerasimov KB (2018) Mater Today Commun 14:77
32. Hu H, Xin JH, Hu H, Chan A, He L (2013) Carbohydr Polym 91(1):305
33. Abureesh MA, Oladipo AA, Gazi M (2016) Int J Biol Macromol 90:75
34. He M, Wang Z, Cao Y, Zhao Y, Duan B, Chen Y, Xu M, Zhang L (2014) Biomacromol 15(9):3358
35. Ashraf S, Asran KR, Neha A, Michler GH, T. Groth (2010) Biomacromolecules 11:3413
36. Cheng Z, DeGracia K, Schiraldi DA (2018) Polymers 10:10
37. Liu JM, Hu SR, Wei CJ, Chen L, Wang J, Liu ZB, Huang XM, Zhu GH (2006) Anal Chim Acta 561(2):198
38. Lu H, Wang W, Wang A (2015) RSC Adv 5(23):17775
39. Qin W, Peng C, Wu J (2017) Ceram Int 43(1):901
40. Zeng T, Li D, Jiang X, Qiu W, Chen Q, Zhang J (2016) J Water Process Eng 12:105
41. Bae H, Yang H, Chung YC, Yoo YJ, Lee S (2014) Bioprocess Biosyst Eng 37(6):1115
42. Xu X, Liu G, Wang Y, Zhang Y, Wang H, Qi L (2018) J Environ Sci (China) 64:317
43. Keller AH, Kleinsteuber S, Vogt C (2018) Microbial Ecol 75(4):941
44. Sheng S, Liu B, Hou X, Liang Z, Sun X, Du L, Wang D (2018) Int Biodeterior Biodegrad 127:26
45. Zhang QQ, Yang GF, Sun KK, Tian GM, Jin RC (2018) Chem Eng J 348:503